# High- and low-field dielectric characteristics of dielectrophoretically aligned ceramic/polymer nanocomposites

V. Tomer,[1] C. A. Randall,[1,a)] G. Polizos,[2] J. Kostelnick,[2] and E. Manias[2]
[1]*Materials Research Laboratory, The Pennsylvania State University, University Park, Pennsylvania 16802, USA*
[2]*Department of Materials Science and Engineering, The Pennsylvania State University, University Park, Pennsylvania 16802, USA*

(Received 24 September 2007; accepted 2 December 2007; published online 13 February 2008)

Polymer/ceramic composites with controlled spatial distribution of fillers are synthesized, and the corresponding changes in their properties are studied. Using dielectrophoretic assembly, we create anisotropic composites of aligned $BaTiO_3$ particles in silicone elastomer and study their electrical properties as a function of ceramic volume fraction and composite morphology. These structured composites show an increase in the permittivity compared to composites with the same composition and randomly dispersed (0–3) fillers. This study emphasizes the important role of conductivity, permittivity, and, particularly, local cluster distribution in controlling high-field dielectric behavior. Designed anisotropy in dielectric properties can provide unexampled paradigms for the development of high energy density materials and gain important insights into the mechanisms that control dielectric breakdown strengths and nonlinear conduction at high fields in polymer/ceramic composites. © *2008 American Institute of Physics*. [DOI: 10.1063/1.2838481]

## I. INTRODUCTION

The development of high energy density storage systems with reduced size is highly demanded in many applications, e.g., consumer electronics, space-based and land-based pulsed power applications, commercial defibrillators, etc.[1] The electrostatic energy density that can be stored in a material is directly proportional to its dielectric permittivity at the local field and the square of the operational electric field. This necessitates that modern materials for high energy density should not only posses high dielectric permittivity, but also provide high operational electric fields with low dissipation factors. The apparent absence of one single-phase material exhibiting such a combination of properties emphasizes the need to integrate two or more materials with complimentary properties, thus, in turn, creating a composite with performance far better than that of its constituents. Ferroelectric oxides have high dielectric permittivity, but suffer from low dielectric strengths. Polymers, on the other hand, have high breakdown field tolerances, but are limited to low dielectric constants. A diphasic composite consisting of these two could provide a material with high dielectric constant[2] and high breakdown field, affording high storage density for a given thickness. The properties of such composites can be tailored through material selection and composition, as well as through percolation and connectivity of phases present within.[3–6] Recent efforts to obtain high energy density materials have primarily focused on randomly dispersed nano- or micron-sized ceramic particulates in a polymer matrix. However, the low dielectric constant of the polymer matrix (usually below 10) limits the maximum possible dielectric constant for reasonable ceramic loadings in the composite. An increase in the filler (ceramic) fraction increases the dielectric constant but introduces problems associated with brittleness, porosity, and low breakdown fields. Many properties such as permittivity, dielectric response, and electrical conduction are greatly influenced by the size, shape, and concentration of inclusions and, most notably, by the geometric arrangement of constitutive phases. Therefore, by properly manipulating these parameters, one can design a unique anisotropic composite with desired properties.

Dielectrophoretic assembly[5–7] can be used to align randomly dispersed fillers into chainlike particle structures by using uniaxial electric fields, thus creating anisotropic composites. These field-structured composites consisting of the filler arranged in pearl chainlike structures demonstrate higher permittivities in the direction of structuring field ($z$-axis) when compared to a randomly dispersed system for the same loading of the filler material. The high dielectric constant of these materials at relatively low filler concentrations may be useful for high energy density material development, but only if they also demonstrate high breakdown fields. An issue of central importance in the improvement of advanced composites is to quantify the dependence of macroscopic properties on the microscopic composite structure. Analytical solutions based on first principles, i.e., Maxwell's equations, can be employed to obtain macroscopic dielectric behavior,[8,9] but it becomes a formidable task in the general case of spatially random composite structures. Pseudo-one-dimensional systems (cf. structured composites) may provide an undemanding way to study polymer-ceramic interactions and the effect of local structure on the macroscopic properties of the composite. Despite marked advances in composite research, there still exists a lack of experimental data probing the dependences of electrical properties on the morphology and connectivity of the constitutive phases. The focus of this paper is to precisely engineer a connectivity pattern within a

a)Author to whom correspondence should be addressed. Electronic mail: car4@psu.edu.

 

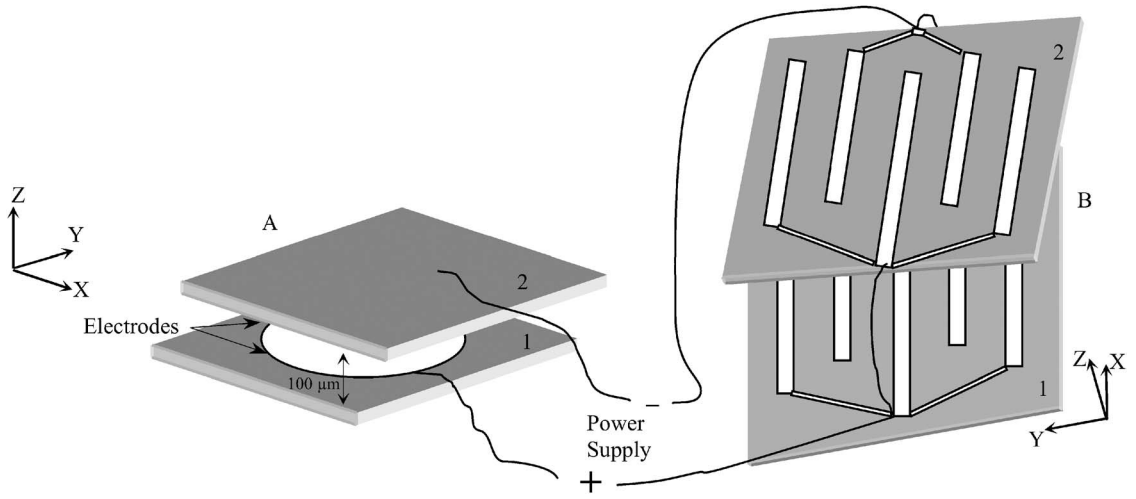


FIG. 1. Schematics of the apparatus used for structuring composites. (A) shows the assembly used for *z*-alignment or 1-3 parallel composites, and (B) indicates the arrangement used for *x*-*y*-aligned or 1-3 perpendicular composites. Plate 2 in (B) is flipped 180° horizontally to give a better perspective of the electrode assembly. Polymer/ ceramic mixtures were squeezed, with the help of a heavy load, between the two plates. Four 70–80 $\mu$m spacers are used to control the thickness of the composites.

polymer/ceramic composite, and further investigate the effect of this directional anisotropy on its electrical properties as a function of filler volume fraction.

This remainder of this paper is organized as follows. In Sec. II, we summarize the experimental approach and materials selection. In Sec. III, we present the results of the dielectric behavior of these composites measured at low electric field conditions. Also, we investigate the performance of our composites, i.e., space charge and losses present, when operated under large external fields. Finally, the conclusions and summary of the paper will be presented in Sec. IV.

## II. NOMENCLATURE

The usual notation 0-3, 1-3, etc., composites follow the nomenclature given by Newnham.[10] Specifically, a 0-3 composite denotes a randomly dispersed filler in a three dimensionally uniform matrix. A 1-3 composite stands for a filler arranged in one dimension in a three dimensional matrix. The 1-3 composites with fillers aligned in the direction of the measuring field (*z*-axis) are noted as *z*-aligned composite, while *x*-*z*-aligned composites refer to fillers aligned perpendicular to the measuring field.

## III. EXPERIMENTAL

### A. Materials

Sylgard184® silicone elastomer from Dow Corning, USA, is chosen as the principal matrix since it has relatively low conductivity and cross-links to a uniform solvent-free system. It is a two part system comprising of a base and curing agent and contains about 55% dimethylvinylated and trimethylated silica, as quantified by thermogravimetric analysis. This polymer is cured at 80 °C for about 1 h and is used for testing without any additional postcure treatment. Cabot's hydrothermal BT-8 ($BaTiO_3$) powder (Cabot Performance Materials, Boyertown, PA) having a Ba/Ti ratio of 0.998 and a median particle size of 0.19 $\mu$m is used as the filler for this study.

### B. Fabrication of model composites

Polymer/ceramic composite samples are prepared by adding the desired volume fraction of the ceramic particulate filler to resin and dispersing by high shear mixing until no sedimentation or agglomerates are visible. Subsequently, a cross-linker is added and the sample is degassed under vacuum in order to remove air voids that are trapped during the mixing process. The degassed suspension is divided into three equal parts: The first two parts are processed in alignment cells, as shown in Fig. 1, to design structured composites [1-3 parallel (*z* aligned) and perpendicular (*x*-*y* aligned)], while the third is subjected to a similar thermal cycle, but in the absence of an electric field. The cells are connected to a high voltage power supply (Trek Power Amplifier model 620A), utilized to amplify the input signal from a lock-in amplifier (SRS 830), and placed on a hot plate. An electric field (1.6 kV/mm at 100 Hz) is then applied to the suspension, while it is held squeezed between the cell plates, concurrently with the application of heat (the sample temperature is approximately 80 °C) in order to accelerate the curing process. The samples are kept on the hot plate with the field applied, until full cross-linking is obtained (~60–90 min). With the help of a charge amplifier, *in situ* capacitance and loss measurements are performed to monitor the alignment during the curing of the composite.

Structured 1-3 composites fabricated using dielectrophoretic assembly[3–7] require high-amplitude alternating electric field to be applied to the polymer/ceramic suspension to avoid electrophoretic transport, space charge accumulation, and electrochemical reactions at the electrodes. The resultant structures, pearl or fibril chain, arise from the time average dielectrophoretic force (DEPF).[11] Without considering higher order terms due to nonlinear effects, the DEPF is expressed as[12]

$$\langle \mathbf{F}_{\mathrm{DEP}}(t) \rangle = 2\pi\varepsilon_m' R^3 \,\mathrm{Re}[K^*(\omega)]\, \nabla E_{\mathrm{rms}}^2,$$

where $\varepsilon_m'$ denotes the medium's (silicone elastomer) real part of the permittivity function, $\varepsilon^*(\omega) = \varepsilon'(\omega) - j\varepsilon''(\omega)$, $R$ the

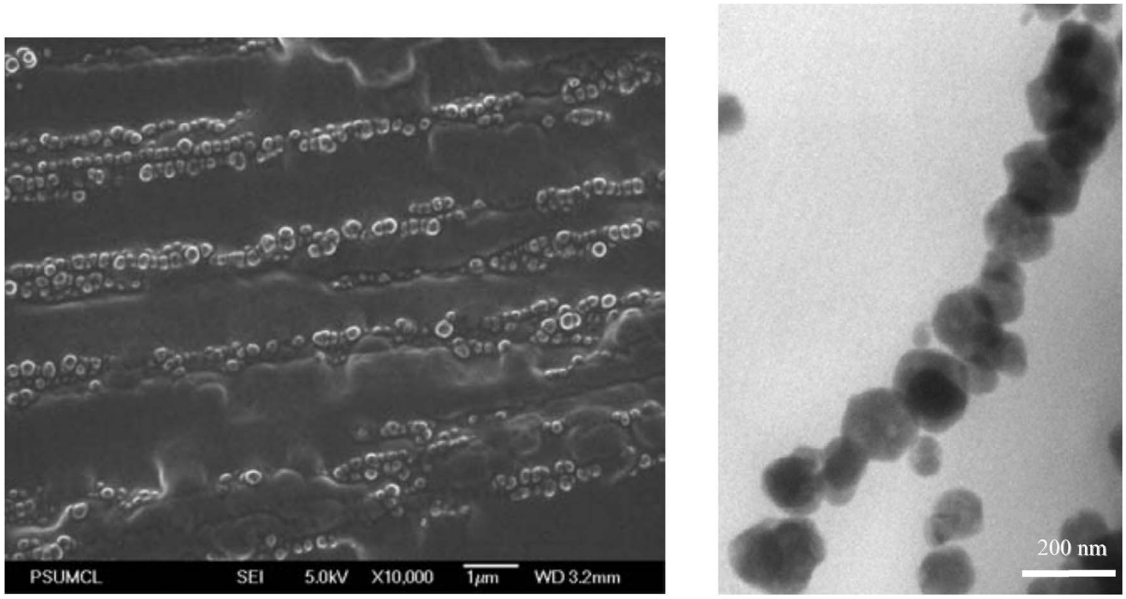


FIG. 2. SEM (left) and TEM (right) micrographs of aligned $BaTiO_3$ (10 vol %) particles in cured polydimethyl siloxane. A 1.6 kV/mm ac field at 100 Hz is used for alignment. The frequency is chosen to minimize the space charge at the electrodes that screens the applied field and to limit electrophoretic transport of the filler phase (Refs. 3, 4, and 6).

particle's radius, $E_{\mathrm{rms}}$ the rms (root mean square) amplitude of the applied field, and $K^*(\omega)$ the complex Clausius–Mossotti function that can be analytically written as

$$K^*(\omega) = \frac{\varepsilon_p^* - \varepsilon_m^*}{\varepsilon_p^* + 2\varepsilon_m^*}.$$

For both the particle and the medium ($i=p,m$), the complex permittivity functions are interpreted in the general form, including also the direct current (dc) conductivity $\sigma_{\mathrm{dc}}$ contribution: where $j=-1$.

### C. Characterization

Scanning electron microscopy (SEM) (Hitachi S-3500N) samples are prepared by fracturing in liquid nitrogen, while a Leica Ultracut UCT microtome with cryoattachment is used for sectioning transmission electron microscopy (TEM) (Joel 2010 $LaB_6$ 200 kV) specimens. Low-field effective permittivity and frequency dependence of the composite are measured by using a Hewlett Packard 4294A and a Novocontrol $\alpha$-analyzer, respectively. High-field polarization–electric field loops are recorded with the help of a modified Sawyer-Tower. All samples are subjected to two successive sine waves, with frequency of 1 Hz, and polarization–electric field loops are plotted with data from the second cycle.

## IV. RESULTS AND DISCUSSION

Composite films with volume percentage of ceramic ranging from 5% to 25% were characterized by SEM and TEM, showing a good filler dispersion within the composite. An excellent alignment is observed, well-defined particle chains with individual particles separated by a small distance (~20 nm), in spite of the small $BaTiO_3$ particle size, as shown in Fig. 2. At higher loadings, due to the strong dipole interactions between the polarized $BaTiO_3$ spheres, a more pronounced particle aggregation is observed, giving rise to a columnlike alignment structure.

### A. Low-field characterization

For the electrical characterization, the films were cut into small square (1 $cm^2$) pieces; a gold circular electrode is sputtered in the center of the top surface, while the bottom was completely electroded. Fringing field effects were minimized by keeping the electrode diameter to a thickness ratio of the order of $10^3$.

The experiment values of the effective permittivity for 0-3 are summarized in Fig. 3(a), along with the theoretical predictions according to various models.[13] The best fit to the experimental data obtained by the model of Wakino *et al.*, considers the influence of dielectric and/or infringing of the electric flux due to discontinuity at the boundary of constituent phases[14] and is given by the expression

$$\varepsilon_r = \exp[\ln\{V_c\varepsilon_c^{(V_c-V_0)} + (1-V_c)\varepsilon_p^{(V_c-V_0)}\}/(V_c - V_0)], \quad (1)$$

where $V_c$ is the ceramic volume fraction, and $\varepsilon_c$ and $\varepsilon_p$ are the ceramic and polymer permittivities, respectively. $V_0$ is the critical volume fraction corresponding to the point of intersection of the logarithmic and Wakino mixing models and is found to be 0.39.

Figure 3(b) shows that for any filler concentration, the 1-3 parallel ($z$ aligned) composites have the highest permittivity while the permittivity difference of 1-3 perpendicular ($x$-$y$ aligned) and 0-3 (random) is relatively small. This anisotropy difference in the effective permittivities is found to increase with the ceramic filler content. Interestingly, the $x$-$y$-aligned samples exhibit slightly higher permittivities than the corresponding randomly dispersed (0-3) composites; this is in contrast to established existing theoretical models that predict the permittivity of 0-3 to fall in between the

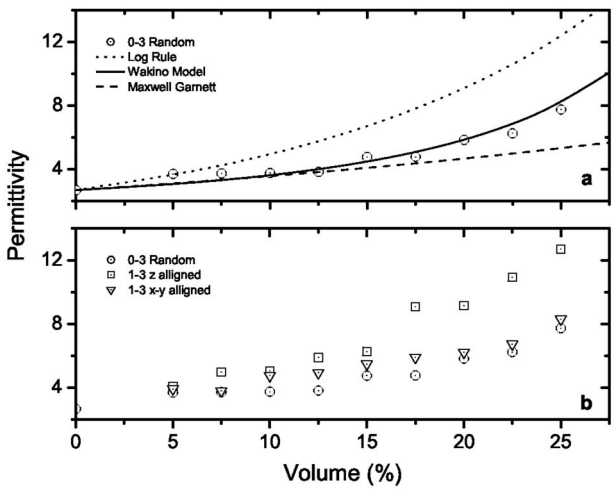


FIG. 3. (a) Permittivity values vs filler volume fraction for the randomly dispersed system; fitting curves derived by using various models are also indicated on the plot. (b) Permittivity values at parallel and perpendicular directions compared to the randomly dispersed composite morphologies. The 1-3 parallel ($z$-aligned) composite shows an increase in permittivity compared to the 0-3 (random), whereas the 1-3 perpendicular ($x$-$y$-aligned) systems show comparable permittivity values.

values of $x$-$y$- and $z$-aligned composites. One explanation for this deviation lies in the mean field nature of such models, where mixing equations reflect a weighted average of the permittivity values over the volume fractions and geometry of the corresponding constituents/phases,[8–15] assuming a perfect periodic structure with each layer's permittivity being described by conventional mixing laws.[16] In aligned composites, the electric field density varies locally, and a more comprehensive approach of the field propagation is needed, so as to account for the contributions of the scattered fields due to the spatial distribution of fillers.[17] Specifically, in order to calculate an average macroscopic field, periodic polarization densities should be taken into account at the microscopic level. This would necessitate the estimation of contributions of the local field distribution, internal microstructure, and multipole interactions on polarizability, which are not typically considered in most of the theoretical models. At this time, this is beyond the goals of this paper.

The frequency dependence of the complex permittivity function is shown in Figs. 4(a) and 4(b). For the data analysis, a superposition of a Havriliak–Negami (HN) expression and a conductivity contribution was employed,[18,19]

$$\varepsilon^*(\omega) = \varepsilon_\infty + \frac{\Delta\varepsilon}{[1+(j\omega\tau_0)^{1-\alpha}]^\beta} - j\frac{\sigma_0}{\varepsilon_0}\omega^{-s}. \tag{2}$$

Least-squares fitting was carried out concurrently for the real and imaginary parts, yielding best values for the common parameters ($\Delta\varepsilon$, $\tau_0$, $\alpha$, and $\beta$),

$$\varepsilon'(\omega) = \varepsilon_\infty + \Delta\varepsilon\frac{\cos(\beta\varphi)}{\left[1+2(\omega\tau_0)^{1-\alpha}\sin\left(\frac{1}{2}\alpha\pi\right)+(\omega\tau_0)^{2(1-\alpha)}\right]^{\beta/2}}, \tag{3}$$

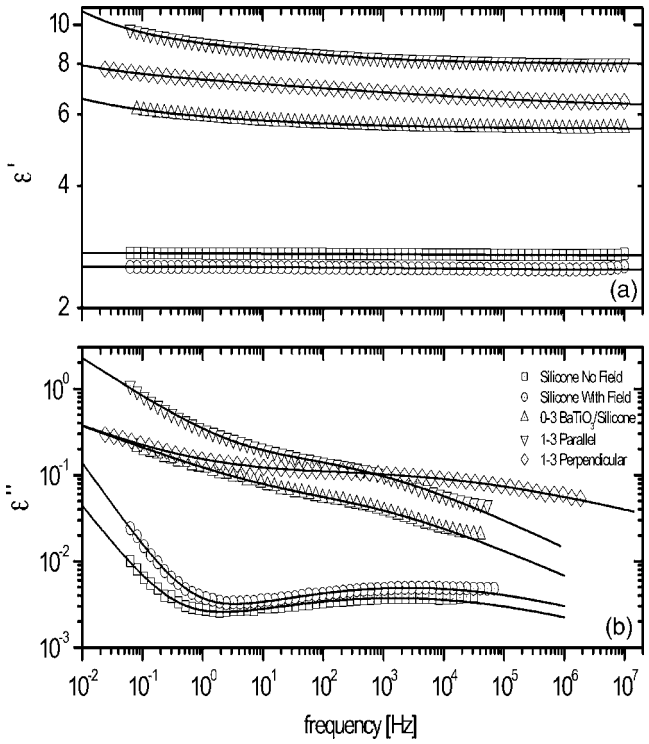


FIG. 4. (a) Frequency dependence of the real part of the complex permittivity function at 20 °C for the 22.5 vol % composites and the polymer matrix (exposed and not exposed to the high electric field used for the particle alignment). The lines are the best fit of Eq. (3) to the data. (b) The corresponding dielectric loss plot describing the interfacial polarization effects. The experimental data are fitted according to Eq. (4) and the parameters are presented in Table I.

$$\varepsilon''(\omega) = \Delta\varepsilon\frac{\sin(\beta\varphi)}{\left[1+2(\omega\tau_0)^{1-\alpha}\sin\left(\frac{1}{2}\alpha\pi\right)+(\omega\tau_0)^{2(1-\alpha)}\right]^{\beta/2}} + \frac{\sigma_0}{\varepsilon_0}\omega^{-s}, \tag{4}$$

where

$$\varphi = \arctan\left[\frac{(\omega\tau_0)^{1-\alpha}\cos\left(\frac{1}{2}\alpha\pi\right)}{\left[1+(\omega\tau_0)^{1-\alpha}\sin\left(\frac{1}{2}\alpha\pi\right)\right]}\right]. \tag{5}$$

In the above equations, $\omega$ is the angular frequency, $\Delta\varepsilon=\varepsilon_s-\varepsilon_\infty=2/\pi\int_0^\infty\varepsilon''(\omega)d\ln\omega$ is the contribution of the orientation polarization to the dielectric function (relaxation strength), with $\varepsilon_s$ and $\varepsilon_\infty$ defining the low and high frequency limits of the $\varepsilon'(\omega)$, and $\sigma_0$ is the conductivity contribution (corresponding to dc conduction for $s=1$). The shape of the loss peak is described by the $\alpha$ and $\beta$ parameters, which are associated with the slopes of the $\varepsilon''(\omega)$ function at the low and high frequency limits with respect to the maximum frequency of the mode,[20]

$$0 \leqslant \alpha < 1, \quad 0 < (1-\alpha)\beta \leqslant 1, \quad (1-\alpha) = \left.\frac{\partial\ln\varepsilon''}{\partial\ln f}\right|_{\omega\ll 1/\tau_0} \quad (1-\alpha)\beta = -\left.\frac{\partial\ln\varepsilon''}{\partial\ln f}\right|_{\omega\gg 1/\tau_0}, \tag{6}$$

where $\tau_0(=1/2\pi f_0)$ is a characteristic time with a value close to the relaxation time $\tau_{\max}$ corresponding to the loss peak maximum frequency,[21,22]

TABLE I. Shape parameters ($\alpha,\beta$) and relaxation strength $\Delta\varepsilon$ values derived from the fitting analysis according to Eqs. (3) and (4) for the dipolar components of Fig. 4. The measured values of ac conductivity at $10^{-1}$ Hz are also listed.

| Sample | $\alpha$ | $\beta$ | $\Delta\varepsilon$ | $\sigma_{ac}$ (S/cm) at $10^{-1}$ Hz |
|---|---|---|---|---|
| Silicone (no field) | $0.77\pm0.01$ | 1 | $0.04\pm0.01$ | $3.76\times10^{-16}$ |
| Silicone (with field) | $0.76\pm0.01$ | 1 | $0.05\pm0.01$ | $8.74\times10^{-16}$ |
| 0–3 $BaTiO_3$/silicone | $0.65\pm0.03$ | 1 | $0.15\pm0.02$ | $1.14\times10^{-14}$ |
| 1–3 parallel | $0.66\pm0.01$ | 1 | $0.76\pm0.01$ | $4.76\times10^{-14}$ |
| 1–3 perpendicular | $0.78\pm0.02$ | $0.75\pm0.08$ | $1.14\pm0.06$ | $1.35\times10^{-14}$ |

$$\tau_{\max}=\tau_o\left[\frac{\sin[(1-a)\beta\pi/(2+2\beta)]}{\sin[(1-a)\pi/(2+2\beta)]}\right]^{1/(1-\alpha)}. \quad (7)$$

The optimum fitting to the data, regarding the dipolar components, was obtained by a Cole–Cole dielectric function for the matrix, as well as for the 0-3 and 1-3 parallel ($z$-aligned) composites, all indicating a symmetric loss peak. In the case of the 1-3 perpendicular ($x$-$y$-aligned) composites, the relaxation becomes asymmetric and is described by the HN function. According to the fitting parameters (summarized in Table I), the relaxation strength $\Delta\varepsilon$ of the matrix is negligible (weak contribution of ionic impurities), and no structural changes are observed after exposing the matrix to similar levels of electric fields as used for filler alignment. However, all the composites exhibit relaxations that can be naturally ascribed to polarization effects at the polymer/ceramic interface. Notably, the structured composites exhibit higher relaxation strength $\Delta\varepsilon$ values when compared to 0-3. Assuming that the number of relaxing units is the same in all the configurations, this behavior can be ascribed to a mean dipole moment enhancement, on average, resulting from the surrounding dipole moment interactions.

Interestingly, the shape parameters shown in Table I and the slopes at the low and high frequency limits, as described in Eq. (5), indicate similar symmetric broadening for the 0-3 and the 1-3 parallel ($z$-aligned) composites, whereas for the 1-3 perpendicular this broadening is asymmetric and more pronounced. This effect may arise from the more heterogeneous local environments at the perpendicular direction, as indicated in the SEM and TEM images of Fig. 2, thus leading to a broader distribution of relaxation times.

In the low frequency region, true dc conduction cannot be identified ($s<1$). In terms of localized mobility (subdiffusion/ac conductivity), the power law contribution is higher in all the composites compared to the pure matrix, as can be seen in Fig. 4(b). The 1-3 parallel ($z$-aligned) composite exhibits higher values of ac conductivity (Table I) than the 1-3 perpendicular ($x$-$y$ aligned), indicating a better formation of percolation paths in the parallel direction and an increase in the anisotropy of conductivity and permittivity.

### B. High-field characterization

The dependence of the electrical properties of filled composites on the applied electric fields is well established.[23] As filler particles become points of local field increase, due to the large contrast between permittivity and conductivity at the filler-matrix interface, it is crucial to understand the high-field losses present in the system arising due to the various contributions, i.e., dc conduction and space charge. The shape of polarization–electric field loops can be used to quantify the behavior of these systems at high fields. Also, both the breakdown strength and the amount of recoverable energy stored should directly depend on the hysteresis phenomena exhibited by these ferroelectric ceramic-powder filled composites.

A series of displacement–electric field ($D$-$E$) loops comparing the polymer matrix and various composites is presented in Fig. 5. The widening (or opening) of loops shows a deviation from the linear behavior of dielectric displacement with electric field ($D=\varepsilon_0\varepsilon' E=\varepsilon_0 E+P$, where $P$ is the polarization) and can be related to the losses present in the system. A linear behavior of polarization with applied field was observed in the $BaTiO_3$-free matrix at all field levels. As expected, the 1-3 parallel ($z$-aligned) composites show the highest losses, at any given volume fraction, when compared to 0-3 or 1-3 perpendicular ($x$-$y$-aligned) composites. This behavior can arise from the development of large local fields in the gap between neighboring $BaTiO_3$ particles in the $z$-aligned composites. Many factors, i.e., dissociation of molecules in the points of increased local field, surface and bulk ionic contaminations in hydrothermally processed ceramic powders, orientation of electric moments of ferroelectric domains, etc., can all contribute to an increase in conductivity and thus create high losses at large fields.[24] On the other hand, the origins of low losses present in the 1-3 perpendicular ($x$-$y$-aligned) composites are not intuitively expected, and more experimental work is required.

It is important to note that with increasing electric field, for each volume fraction, the amount of recoverable energy is increasing. However, the losses present in the 1-3 parallel ($z$-aligned) system compete with the advantages of increased permittivity. The slope of $P$-$E$ loops can be used to calculate the values of permittivities at high fields. The required equations to quantify the real and imaginary parts of the complex dielectric permittivity are summarized in Table II. By associating the area inside the hysteresis loop to the imaginary part of permittivity and using Table II, we can calculate the real part of permittivity.[25] The effective $\varepsilon'$ values are found to increase with increasing filler content and electric fields, as shown in Fig. 6. This reaffirms the presence of structural anisotropy even at high fields and further demonstrates the difference in effective permittivity of the three composites. Both $x$-$y$- and $z$-aligned composites show a dependence of permittivity on electric field. On the other hand, pure silicone elastomer with a linear relationship between dielectric displacement and applied electric field, as shown in Fig. 5, does not show this dependence. In this case, the low-field and high-field values were found to be comparable within experimental errors. The difference in behavior of these composites at low and high fields indicates that the interface, relative field enhancement, and local conductivity between the polymer and filler govern the distribution and/or origin of losses, space charge, and conduction present at high fields and low frequencies.

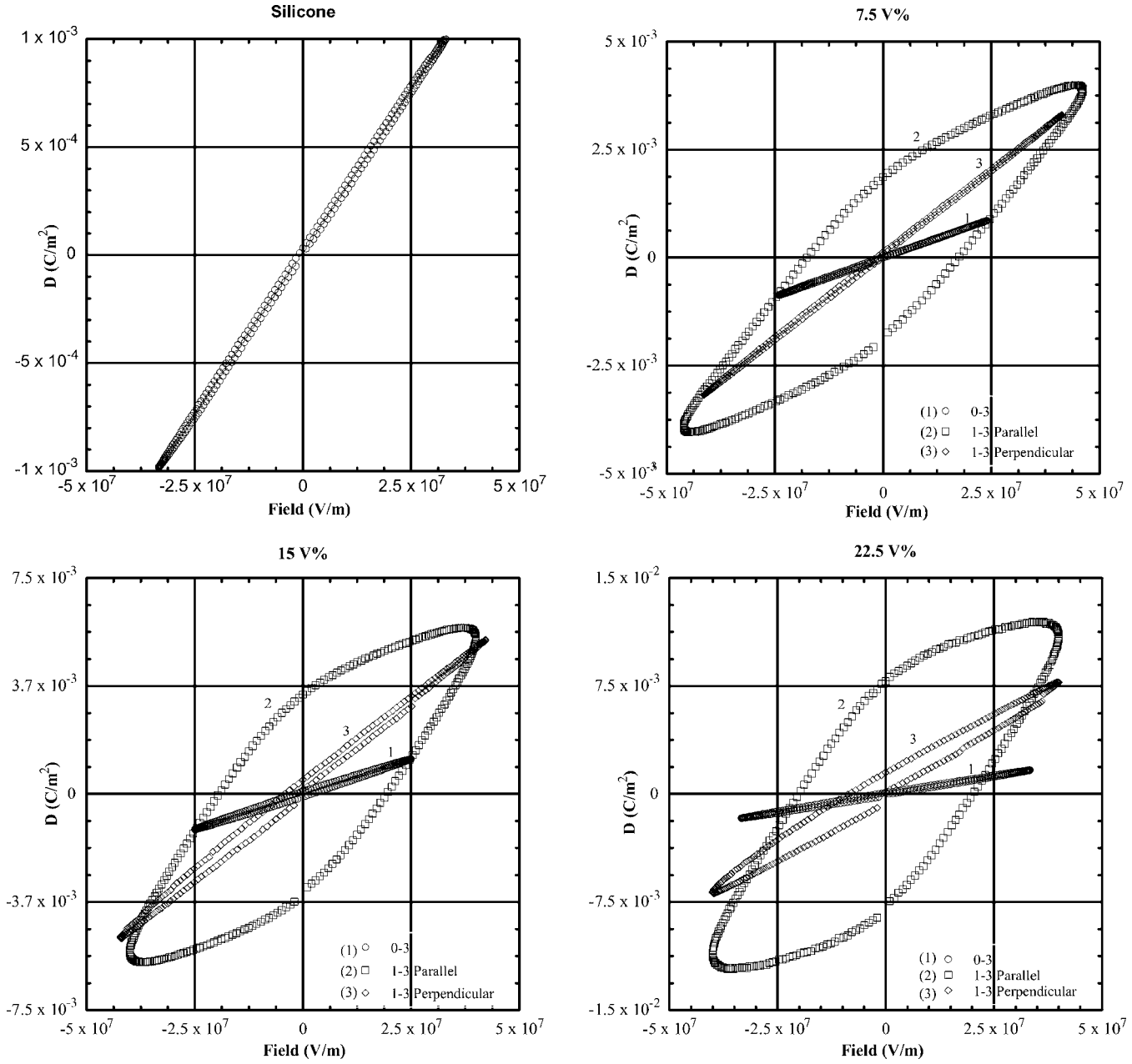


FIG. 5. A comparison between the displacement–electric field loops, obtained at 10 Hz, for various volume fractions of structured and randomly dispersed composites. The *z*-aligned composites clearly indicate higher losses compared to 0-3 and *x*-*y* aligned composites.

## V. CONCLUSIONS

This work demonstrates that by designing the spatial distribution of fillers inside the polymer matrix, one can significantly enhance the dielectric properties of 0-3 composites. The increased values of permittivities in structured composites may provide a platform for obtaining high energy density materials. This anisotropy in permittivity and conductivity can be exploited to design composites with desired properties. However, with an improper choice of matrix and filler, the extra losses present at high fields may compromise any advantages. We are currently investigating the effect of this induced anisotropy on the electrical breakdown characteristics of these composites. Future work will focus on identifying other candidates for polymers and fillers with different shapes and textures, and on developing theoretical models for the permittivity and breakdown mechanisms of such anisotropic composites.

TABLE II. Equations used to separate the real and imaginary parts of high-field complex permittivity obtained through displacement–electric field loops.

| Displacement–electric field loops | | |
|---|---|---|
| Complex permittivity | $\varepsilon^* = D_{\text{p.-p.}}/2E_0$ | $D_{\text{p.-p.}}$: peak to peak displacement ($C/m^2$) |
| Imaginary permittivity | $\varepsilon'' = A_E/\pi E_0^2$ | $A_E$: loop area ($C\,V/m^3$) |
| Real permittivity | $\varepsilon' = \sqrt{\varepsilon^{*2} - \varepsilon''^2}$ | $E_0$: electric field (V/m) |

## ACKNOWLEDGMENTS

The authors would like to acknowledge the Office of Naval Research and MURI-00014-05-1-0541 for financial

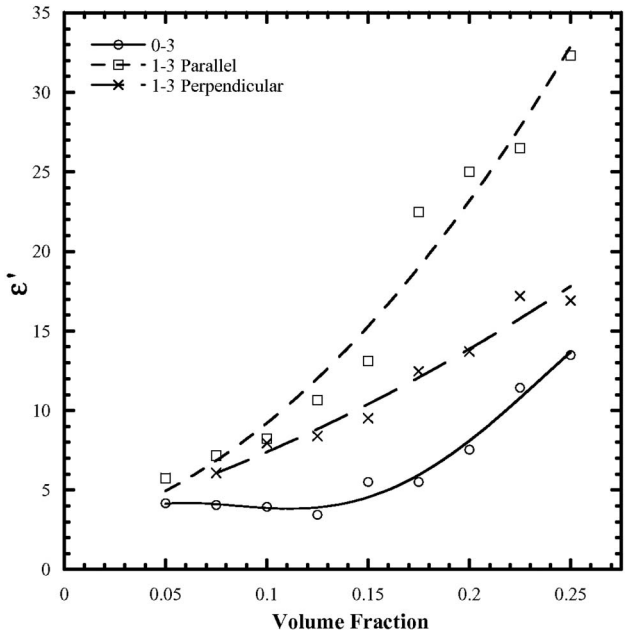


FIG. 6. High-field permittivities calculated using the hysteresis loops and equations provided in Table II. Higher permittivities, when compared to 0-3 or *x*-*y* aligned, are shown by *z*-aligned composites at all volume fractions.

support. They would also like to thank Paul Moses and Jeff Long for their help with the setting of electrical equipment

[1]K. M. Slenes, P. Winsor, T. Scholz, and M. Hudis, IEEE Trans. Magn. **37**, 324 (2001).
[2]C. A. Randall, S. Miyazaki, K. L. More, A. S. Bhalla, and R. E. Newnham, Mater. Lett. **15**, 26 (1992).
[3]C. P. Bowen, T. R. Shrout, R. E. Newnham, and C. A. Randall, J. Intell. Mater. Syst. Struct. **6**, 159 (1995).
[4]C. P. Bowen, R. E. Newnham, and C. A. Randall, J. Mater. Res. **13**, 205 (1998).
[5]J. E. Martin, C. P. Tigges, and R. A. Anderson, Phys. Rev. B **60**, 7127 (1999).
[6]C. A. Randall, D. V. Miller, J. H. Adair, and A. S. Bhalla, J. Mater. Res. **8**, 899 (1993).
[7]S. A. Wilson, G. M. Maistros, and R. W. Whatmore, J. Phys. D **38**, 175 (2005).
[8]B. Sareni, L. Krähenbühl, A. Beroual, and C. Brosseau, J. Appl. Phys. **80**, 1688 (1996); **81**, 2375 (1997).
[9]J. P. Calame, J. Appl. Phys. **99**, 084101 (2006).
[10]R. E. Newnham, Ferroelectrics **68**, 1 (1986).
[11]T. B. Jones, *Electromechanics of Particles* (Cambridge University Press, Cambridge, England, 1995).
[12]H. A. Pohl, *Dielectrophoresis* (Cambridge University Press, Cambridge University England, 1978).
[13]P. S. Neelakanta, *Handbook of Electromagnetic Materials: Monolithic and Composite Versions and Their Applications* (CRC, Boca Raton, FL, 1995).
[14]K. Wakino, T. Okada, N. Yoshida, and K. Tomono, J. Am. Ceram. Soc. **76**, 2588 (1993).
[15]A. Beroual, C. Brosseau, and A. Boudida, J. Phys. D **33**, 1969 (2000).
[16]A. Sihvola, *Electromagnetic Mixing Formulas and Applications* (The Institution of Electrical Engineers, London, 1999).
[17]W. F. Brown, Jr., J. Chem. Phys. **23**, 1514 (1955).
[18]S. Havriliak and S. Negami, J. Polym. Sci., Part C: Polym. Symp. **14**, 99 (1966).
[19]*Broadband Dielectric Spectroscopy*, edited by F. Kremer and A. Schönhals (Springer-Verlag, Berlin, 2002).
[20]A. K. Jonscher, *Dielectric Relaxation in Solids* (Chelsea Dielectric, London, 1983).
[21]F. Alvarez, A. Alegria, and J. Colmenero, Phys. Rev. B **44**, 7306 (1991).
[22]A. Boersma, J. van Turnhout, and M. Wübbenhorst, Macromolecules **31**, 7453 (1998).
[23]C. J. Dias and D. K. Dasgupta, J. Appl. Phys. **74**, 6317 (1993).
[24]D. P. Agoris, I. Vitellas, O. S. Gefle, S. M. Lebedev, and Yu. P. Pokholkov, J. Phys. D **34**, 3485 (2001).
[25]R. E. Eitel, T. R. Shrout, and C. A. Randall, J. Appl. Phys. **99**, 124110 (2006).